F2016-ESYG-018

COMBUSTION AND PARTICULATED MATTER FORMATION IN MODERN GDI ENGINES: A MODELLING STUDY USING CFD

[1]Bonatesta, Fabrizio; [1]Hopkins, Edward; [1]Francavilla, Claudia; [1]Bell, Daniel; [2]La Rocca, Antonino*

[1]Department of Mechanical Engineering and Mathematical Sciences, Oxford Brookes University, UK; [2]Department of Mechanical Materials and Manufacturing Engineering, University of Nottingham, UK.

KEYWORDS – GDI Engine; CFD; Soot Modelling; Soot Sectional Method; Star-CD.

ABSTRACT
Modern GDI engines are efficient power platforms, but produce large quantities of ultra-fine soot particles. Fuel mal-distribution and, in some cases, liquid fuel film are commonly addressed as the primary causes of particulate matter formation. Multi-dimensional engine modelling can be used effectively to gain an improved understanding of the in-cylinder processes leading to particulate matter. The work presented here investigates soot mechanisms in a modern wall-guided GDI engine using commercial CFD software Star-CD. Two part-load operating conditions are investigated, 2300 rev/min - 60 Nm, and 2300 rev/min - 120 Nm. The multi-stage semi-empirical Soot Sectional Method is used to simulate the physical and chemical in-cylinder mechanisms leading to soot emissions.

The results of the simulations show better mixture preparation in the high load case, mostly on account of enhanced fuel atomisation and stronger mixing. The lower load case features wider mixture stratification, with a more confined, lower temperature burning zone. In both cases, a strong temperature drop establishes between the hot core and the cylinder walls. Higher levels of oxygen correspond to regions of lower temperature near the walls and vice-versa. This unfavourable arrangement, compounded to the lack of mixture homogeneity, leads to high levels of EVO soot in the lower engine load case.

TECHNICAL PAPER

1. INTRODUCTION

In the last two decades, there has been rapid and significant development concerning internal combustion engine technology and this has led to improved performance and efficiency [1]. Gasoline Direct Injection (GDI) engines are comparatively efficient power platforms, but the increased understanding of emission implications upon public health [2] and the environment poses reasonable concerns upon the long-term viability of this technology. Requirements of the Euro 6 regulations impose limitations to particulate numbers ($6.0x10^{11}$ particles per km) for post July 2017 vehicles. Most engine and car manufacturers are currently engaged in a serious debate on whether improved control strategy would be sufficient, without the use of Gasoline Particulate Filters (GPF), for compliance with proposed standards. With 2017 marking the introduction of the new transient Real Driving Emissions (RDE) emission testing, it is acknowledged that much developmental work must be completed if these standards are to be met.

The shift from gasoline Port-Fuel Injection (PFI) engines to direct injection has been observed to produce increased soot emissions, something that, until recently, has predominantly been associated with CI diesel engines. The level of understanding of particulate emissions in CI engines is relatively well developed in comparison with that of GDI systems. Recent experimental work has allowed the variation in particulate matter emissions to be monitored for the GDI engine. The available literature shows that particulate matter formation is linked to incomplete air-fuel mixing, coupled with wall wetting effects [2-6]. Other studies, such as the one undertaken by Hageman and

Rothamer [7], have indicated that a significant number of small particles are produced even under stoichiometric or lean operation, with diameters of less than 50 nm. Whilst experimental testing allows some level of understanding of particulate formation, there is compelling evidence that alternative methods are necessary to enable a more fundamental comprehension of the relevant mechanisms.

If appropriately calibrated, 3D Computational Fluid Dynamics (CFD) modelling provides valuable insight into in-cylinder chemical and physical mechanisms leading to particulate formation [8, 9], and may help towards an improved understanding upon the influence of engine variables. The present work aims to contribute to the novel area of soot modelling in GDI engines. Specific focus has been given to the potentials and limitations of the current modelling approaches, with a view to facilitate further research in the field.

2. METHODOLOGY

The simulations were carried out for the arrangements of a 4-stroke, 4-cylinder, central-spark plug pent-roof design, Euro 4 standard, GDI engine used in parallel experimental studies. The engine featured wall-guided injection system, with side-mounted 7-hole high-pressure fuel injectors. This section focuses on CFD methodologies; details of engine testing and of engine-out particulate matter measurement methodology can be found in reference [10].

2.1 Spray Modelling Methodologies and Calibration

Spray modelling for a GDI engine is of upmost importance as the injection and subsequent wall-impingement bear a strong effect on the process of mixture preparation, combustion and hence pollutant formation. Due to its comprehensive nature, in this work the Kelvin-Helmholtz and Rayleigh-Taylor (KH-RT) model is used for spray simulation [11]. The primary breakup is governed by so called Kelvin-Helmoltz instabilities, best explained by Malaguti et al. [12]; the concept of Rayleigh-Taylor (RT) instabilities for secondary breakup is based on works of Rosa et al. [13]. A Probability Density Function (PDF) of the Rosin-Rammler type was implemented for fuel droplet initial size distribution, governed by an average droplet diameter and a tuning constant. Following the work of Semião et al. [14] and Huang et al. [15], the average droplets diameter was set to 50 μm and the tuning constant to 3.13. The spray model is based on a discrete method, where a large number of computational "parcels" are employed to represent groups of identical droplets featuring equal geometrical, mechanical and thermo-physical properties. A coupled Lagrangian approach is used for solving sprays within the commercial CFD software Star-CD.

Spray model calibration is based on high-speed camera images obtained from the same GDI injector as used in test engine, carried out at injection pressure of 120 bar within an optical-access vessel in non-evaporative conditions at 1 bar [16]. A static cylindrical computational domain was created to resemble the experimental vessel, counting 155,000 cells with typical size of 2 mm [17]. In the present work, simplified fuel injection profiles of realistic shape have been devised on the basis of the experimental mass flow rate vs time injection data presented by Montanaro et al. [18]. Turbulence within the vessel is modelled via the RNG k-ε model. The injected droplets are subject to the influence of gravity and turbulence dispersion, and exchange momentum and heat with the surrounding gas. The thermo-physical properties of liquid and vapour phases are taken as temperature dependent.

Calibration was carried out in terms of spray morphology, penetration as well as droplets Sauter Mean Diameter (SMD). Calibration required tuning of the KH-RT model constants to control the rate of primary and secondary break-up. A comparison of modelled and experimental sprays showing acceptable morphological resemblance is given below in Figure 1. Excellent agreement was also found in terms of penetration distance, see Figure 2, for the initial part of the injection process where experimental data was available. At the end of injection, the modelled SMD settles to a stable value of approximately 16 μm, which is in good agreement with levels reported for an injection pressure of 120 bar [19, 20].

After the vessel spray validation was completed successfully, analogous spray modelling set-up was implemented within the CFD simulations of the GDI engine cycle. The mechanism of spray/wall interaction was modelled using a Bai-ONERA approach, which is an improvement to the approach due to Bai and Gosman [21], and includes the ONERA model [13] for the higher temperature regime and the effects of surface characteristics. The set up for this model is taken from relevant literature [11].

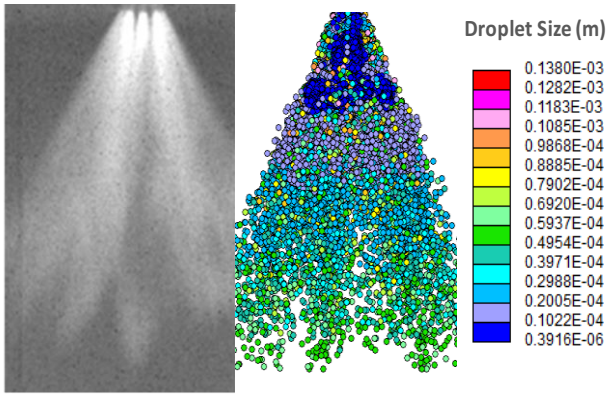

Figure 1. Comparison of modelled and experimental GDI fuel sprays at 320 μs from start of injection. Modelled spray droplets coloured by size in meters.

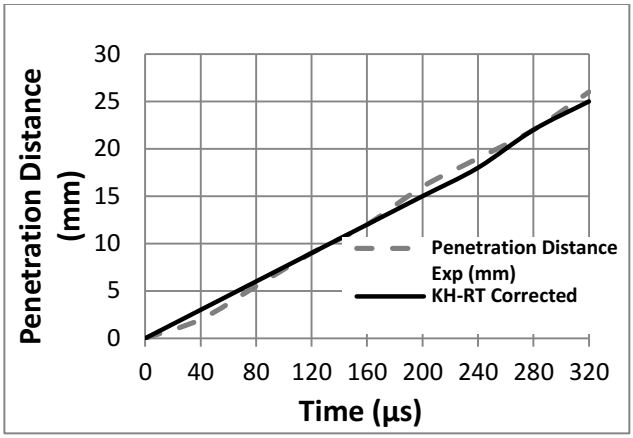

Figure 2. Comparison between experimental and computed spray penetration. Fuel injection pressure: 120 bar; injection duration: 0.32 ms. Penetration calculated as distance between injector nozzle and the bulk of the spray.

2.2 Engine Cycle Modelling Methods

Due to the symmetry of the pent-roof design, only half of the cylinder geometry was considered. The volume mesh was created within the ES-ICE software environment, using a trimming method to yield regular hexahedral cells, coupled with automatic generation of the motion events. The grid featured typical cell size of 1 mm [22] with local refinement in the vicinity of the spark-plug and valve seat areas. A single-cell boundary layer at the walls with typical size 0.3 mm was also implemented. Total cell count was 210 k with piston at Top Dead Centre (TDC), and 360 k with piston at Bottom Dead Centre (BDC).

All engine simulations were carried out within the Star-CD solver. The Monotone Advection and Reconstruction Scheme (MARS) is used for the momentum and turbulence equations; the linear Upwind 2nd order Differencing scheme (UD) is used for the temperature equation, whereas the Central Differencing scheme (CD) for density. As reported in the previous section, the RNG k-ε closure approach is used to model the turbulence and momentum length and scale. Temperature-dependent thermo-physical properties are used for all gaseous components. The fuel model is the "GASOLINE1" model, based on the work by BTU Cottbus/LOGE [23]. This surrogate fuel, treated within the solver as a single component, is based on a Toluene Reference Fuel (TRF) blend, with composition optimised to obtain the correct Lower Heating Value, aromatic content and RON to correspond to commercial EURO 4 gasoline fuel. NIST tables are used to estimate the variation of the fuel thermo-chemical properties as a function of temperature. The fuel used in the parallel soot sampling campaign was a RON 95 reference fuel of fixed composition, showing certified aromatics contents between 29 and 35%.

The general purpose 3-Zone Extended Coherent Flamelet Model (ECFM-3Z) [24] is used here to simulate the process of theoretically-homogeneous, partially-premixed, spark-ignition turbulent combustion. The model considers three computational zones, namely unmixed-fuel zone, mixed-gases zone, unmixed-air plus EGR zone. These are modelled as sub-grid quantities. The mixed zone is where combustion takes place as a result of turbulent molecular mixing between the gases in the other two zones. The diffusion flame calculations are carried out using a Magnussen-type approach [11]. Flame propagation within the mixed zone is modelled via the flame surface density transport

equation. Here, empirical coefficients α and β are used for the purpose of combustion calibration. This was carried out targeting a close match between simulated and experimental CA-resolved pressure curves.

2.3 Soot Modelling Methods

In gasoline partially-premixed combustion, soot particles in the ultra-fine size range (diameters of less than 100 nm) are produced through several chemical and physical processes during and after the combustion process. The main steps can be summarised as follows: production of Polycyclic Aromatic Hydrocarbons (PAH), as a result of oxidation of fuel in oxygen-starving or rich regions; particle inception or nucleation, where PAH species featuring up to four aromatic rings combine to form primary particles; particle growth, including condensation of PAH molecules and surface growth due to interaction with acetylene C2H2 and other species; collision and consequent coagulation/agglomeration, taken as a purely physical mechanism; particle oxidation in presence of oxygen and/or OH radicals, at high temperature, which proceeds for the whole duration of the process.

The most advanced soot model available within Star-CD, called the Soot Sectional Method [25], has been used in this work. This is a semi-empirical multi-stage approach which considers all the relevant mechanisms and their inter-connection. The Sectional Method solves the transport equation for soot mass fraction in each of 20 theoretical particle volume "sections". In order to minimise the computational cost, the soot sources are calculated through tabulated "pre-factors" using available libraries. In this work, the Plug Flow Reactor (PFR) library has been selected and used consistently as it returns realistic in-cylinder soot formation curves, as confirmed by previous optical [26] and simulation work [8, 9]. The pre-factors are calculated as a function of in-cylinder local conditions as well as a fuel segregation variable and a progress variable for combustion. The progress variable constitutes the link between the combustion and the soot sub-models. As reported in [25], an assumption of this model is that the progression of combustion influences the soot chemistry, but not vice-versa.

The original Sectional Method setup available within the Star-CD solver was developed and validated for diesel combustion systems [25, 27]; careful model optimisation was therefore necessary. The limited literature on soot modelling in GDI engines shows that re-adaptation of models and mechanisms originally developed for diesel combustion is common [8, 9, 28]. To the Authors' best knowledge, no literature has been published on the application of the Sectional Method to GDI combustion. The process of re-adaptation must consider the intrinsic differences between GDI and diesel combustion, and translate these into an appropriate balance between the relative weight of the various soot mechanisms. The process of model optimisation used information from relevant sources and a range of calibration factors which were suitably modified to strike a close match between modelled and experimental values of engine-out total number density and mass concentration. For calibration purposes, the chemical composition of the burned gas and dispersed phase after EVO was taken as frozen, enabling a direct comparison between cylinder gas composition at EVO and species measured through exhaust manifold sampling. While common [22], this assumption suffers from uncertainties in regards to condensed volatile fraction [29], presence of metallic compounds [30], or further particle coagulation and oxidation. For these reasons, soot number density values are said be predicted with acceptable level of confidence when within one order of magnitude of experimental levels [27].

2.4 Engine simulation set-up, boundary and initial conditions

All engine cycle simulations were started at 40 CA deg Defore Top Dead Centre (BTDC) (end of exhaust stroke), and ended at EVO of the following cycle. This is a classic setting which allows all the major engine cycle events to be captured. Two part-load engine running conditions were selected for the present work, with engine speed fixed at 2300 rev/min and engine torque of 60 and 120 Nm, respectively. Experimental data from parallel tests were used as initial and boundary conditions for the simulations. The relevant experimental data are summarised in Tables 1 and 2.

Figure 3 uses a mesh-edge image to give further details about simulation setup and boundary conditions in regards to initial wall temperature and gas composition.

Engine Load (torque) Nm	Intake Pressure (Bar)	Exhaust Pressure (Bar)	Intake Temperature (°C)	Exhaust Temperature (°C)
60	0.618	1.080	24.8	547.1
120	0.914	1.133	28.5	686.4

Table 1. Experimental pressure and temperature data, at fixed engine speed of 2300 rev/min.

Engine Load (Torque) (Nm)	Start of Injection (CA deg BBDC)	End of Injection (CA deg BBDC)	Fuel injected (mg/cycle/cyl)	Ignition Timing (CA deg BTDC)
60	122	99	12.80	35
120	125	101	23.33	15

Table 2. Experimental engine fuel consumption, injection and spark ignition advance data, at fixed engine speed of 2300 rev/min.

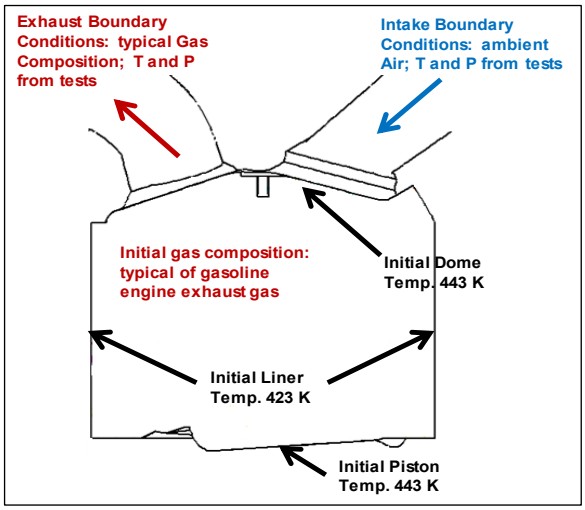

Figure 3. Details on initial wall temperature and gas composition used in all CFD simulations.

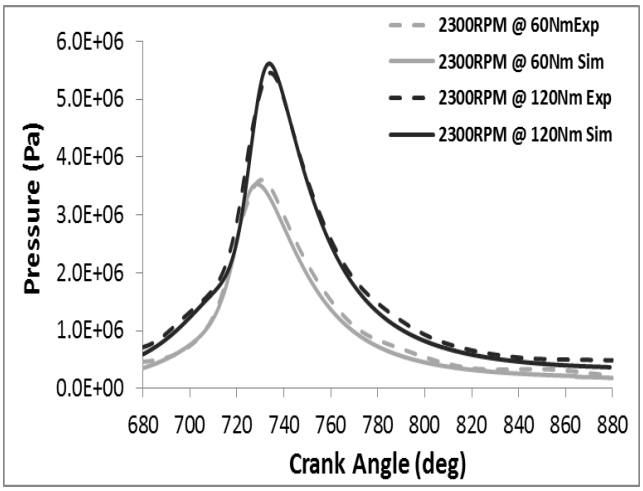

Figure 4. Comparison between modelled and experimental in-cylinder pressure curves for the three engine conditions investigated.

2.5 Combustion and Soot Models Calibration

Figure 4 shows the comparison between modelled and experimental in-cylinder pressure for the operating conditions investigated. Control over tuning factors α and β allows reasonable agreement to be achieved throughout, with the final calibrated pressure traces matching the experimental ones in terms of peak pressure, its location, as well as combustion phasing. Importantly, the simulated data replicate quite well the transition between flame development and rapid burning, as indicated by the change in slope taking place close to TDC, and the rapid burning stage in its entirety. Reportedly, this stage of combustion is the most significant one for the formation of soot in spark ignition theoretically-homogeneous engines [10].

At the current stage of the research project, the identification of a unique calibration setup for the Soot Sectional Method, which delivered accurate predictions across the board, was not viable. Instead, the model was optimised for the higher engine load case, 2300 rev/min - 120 Nm, and then applied without any modifications to the other case. Figure 5 shows the total soot number density and mass concentration histories for the optimised case, and the measured engine-out levels represented at EVO. A logarithmic scale is used for soot number density for clarity of visualisation. The experimental values of number density and mass concentration, measured using differential mobility spectrometry [10], were 1.52×10^{7} #/cc and 0.007 µg/cc, respectively. Acceptable agreement is seen between measured and modelled quantities, which were accurate to within 20%. Number density and mass concentration increase rapidly during the main combustion event reaching maximum levels few CA degrees after peak heat release rate from combustion [26]. Past this point, the mechanism of oxidation becomes dominant and, along with

coagulation/agglomeration, contributes towards lowering levels. Further analysis indicates that particles oxidation, which induces a reduction in total mass, actually ceases between 20 and 30 CA deg past TDC, while particle number continues to decrease due to effects of coagulation.

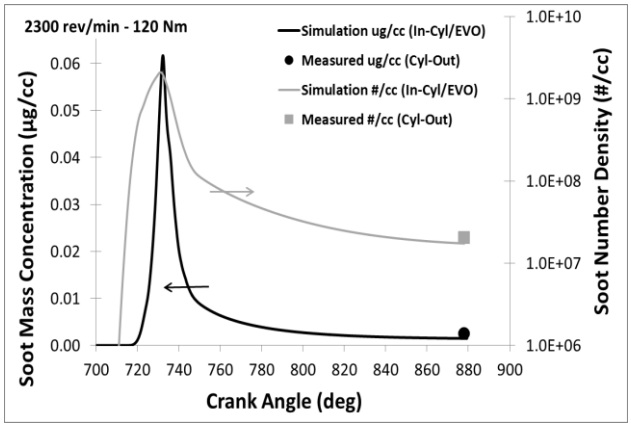

Figure 5. Total in-cylinder number density and mass concentration histories and comparison with experimental engine-out level represented at EVO. Engine operating condition: 2300 rev/min and 120 Nm.

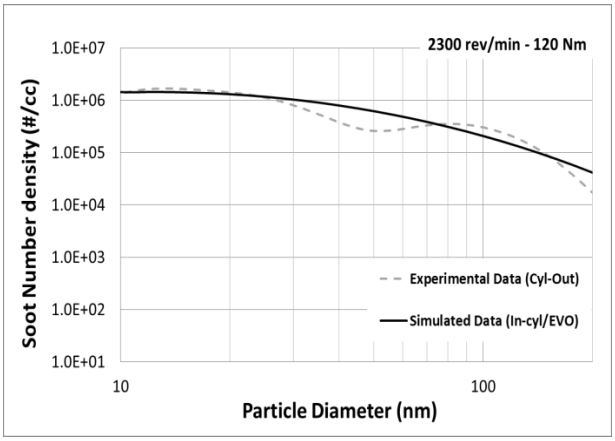

Figure 6. Comparison between experimental and modelled (EVO) engine-out size-resolved soot number density distributions. Engine operating condition: 2300 rev/min and 120 Nm.

The lower engine load case, 2300 rev/min – 60 Nm, produced higher levels of engine-out soot, mostly on account of poorer mixture preparation. Compared to the higher engine load case, number density showed a three-fold increase and mass concentration a two-fold increase. The Soot Sectional Method was able to capture the increasing soot loadings measured in this case, but both modelled quantities were under-estimated. While there is evidence that model tuning is required for specific engine operation, the results of the simulation provide valuable insight into the soot formation mechanisms and are intended to facilitate future high-quality research, and a more intensive use of the approach.

In order to further assess the capabilities of the soot model for GDI theoretically-homogeneous combustion, modelled and experimental size-resolved particle number density distributions were compared for the 2300 rev/min – 120 Nm case, see Figure 6. The experimental curve shows a peak in nucleation mode (particle diameter < 50 nm) corresponding to 13 nm, and a reduced peak in accumulation mode at 85 nm. About 87% of particles are emitted in nucleation mode, and 13% in accumulation mode. The modelled curve follows the experimental one, but the model response is not fully satisfactory as the typical bi-modal nature of GDI-type distributions is not well captured. The model over-predicts the number density in the range 30 to 70 nm. About 93% of particles are modelled in nucleation mode, 7% in accumulation mode. The limited literature available in the field either does not report these curves [9, 28], or the accuracy of prediction is unsatisfactory [8]. The underlying reasons of this poor performance will be object of future investigation.

3. RESULTS AND DISCUSSION

Further results from the simulation work are reported and analysed in this section. The presentation follows the engine cycle and the focus is given to those events which are thought to be more relevant to the process of soot formation.

3.1 Air-Fuel Mixture Formation and Combustion

As expected in a modern, 4-valve, pent-roof chamber design, a typical rotating tumble flow structure establishes in the cylinder with peak gas velocity mid-way through the intake stroke at the time of maximum intake valve lift. The rotating flow has lower strength but remains well identified during the compression stroke. The air-fuel mixing process starts with fuel injection and proceeds until after combustion has commenced [10, 17]. Fuel distribution at spark timing is normally used as a good indicator of the effectiveness of mixture preparation. To this end, Figure 7 shows images of equivalence ratio distribution at spark timing for the two cases investigated. In spite of the early

intake stroke fuel injection, see Table 2, the process of direct injection returns a mixture which is generally not well prepared [2-7, 31]. Much better mixture homogeneity is achieved in the higher load case, where greater injection pressure leads to enhanced fuel atomisation and a slightly stronger rotating flow structure. The lower load case features strong mixture stratification, with rich layers along the cylinder dome, and lean layers along the piston crown. Moving vertically along the spark plug axis, the equivalence ratio shows an adverse variation between 0.75 and 1.4. This variation is amplified in the remote, isolated corners of the combustion chamber. Poor mixture preparation has been addressed as one of the most important factors contributing to high levels of engine-out soot measured experimentally in GDI engines [2-6].

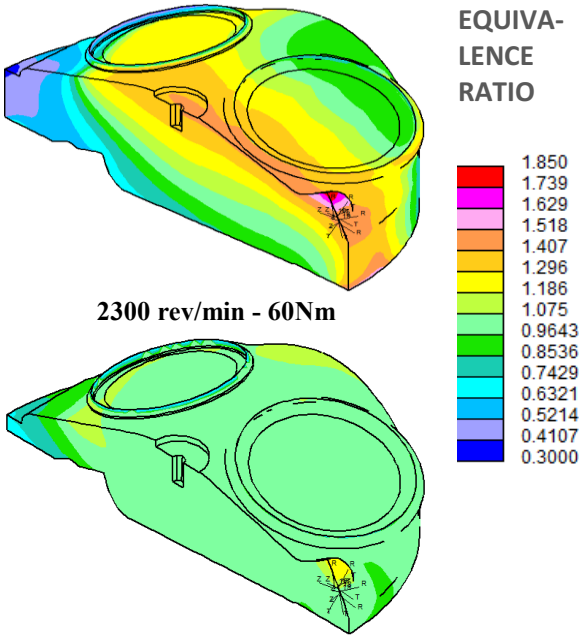

Figure 7. In-cylinder equivalence ratio distribution at spark timing for the two operating conditions investigated.

3.2 Flame Development and Propagation

Symmetry plane temperature distributions at 10% MFB (Mass Fraction Burned) are presented in Figure 8; these provide an indication of the advancement of the turbulent flame front. The 10% MFB is reached at approximately the same CA location, between 4 and 2 CA deg BTDC. This is where soot nucleation becomes important due to availability of Polycyclic Aromatic Hydrocarbons in the high temperature burned gases behind the flame front. The flame kernel develops centrally, and then expands and is deformed (mostly elongated) by the prevailing counter-clockwise rotating flow. The core temperature level increases as expected with engine load. Interestingly, the fuel-rich layers which establish along the cylinder dome in the lower load case, force combustion to develop in the lower, near-stoichiometric part of the chamber.

Figure 9 shows temperature contours at 90% MFB. In the higher load conditions, the rapid burning angle (CA interval between 10 and 90% MFB) stretches for approximately 16 CA deg. In this case, maximum combustion temperature of about 2900 K is reached at 16 CA deg After Top Dead Centre (ATDC). Combustion is slightly slower and at lower temperature for the lower engine load conditions; peak combustion temperature of 2750 K is reached at 9 CA deg ATDC, the rapid burning angle is approximately 18 CA deg. Importantly, all conditions investigated show a dramatic drop in temperature moving from the hot burned gas core to the cylinder walls, where due to heat transfer the temperature remains between 700 and 800 K. Residence of the formed soot particles in the chamber periphery during the expansion stroke, may lead to low levels of soot oxidation.

3.3 Soot Modelling

The Soot Sectional Method associates the local rate of PAH formation to the rate of particle inception, whereas growth relates to condensation of PAH onto existing particles and to surface growth by combination with acetylene and other species. Ultimately, it is seen that the rate of production of precursors and growth species is proportional to local fuel concentration. Figure 10 shows the distribution of fuel concentration, in terms of mass fraction, at three cycle locations: at 10 CA deg ATDC, which is approximately where soot formation reaches its apex; at 40 CA deg ATDC, where all soot mechanisms and combustion are about to end; at EVO timing. Isomeric views have been chosen for improved visualization. From 10 CA deg ATDC and on to EVO, the level of residual fuel within the combustion chamber reduces due to combustion; as expected, higher fuel concentration corresponds to regions of lower temperature near the walls. From 40 CA deg ATDC, the leftover fuel in the higher engine load case is located mostly in the chamber periphery, and along the liner walls. Legacy of poor mixture preparation, the lower engine load case

conserves an ample strip of sub-stoichiometric mixture along the dome up until the end of combustion.

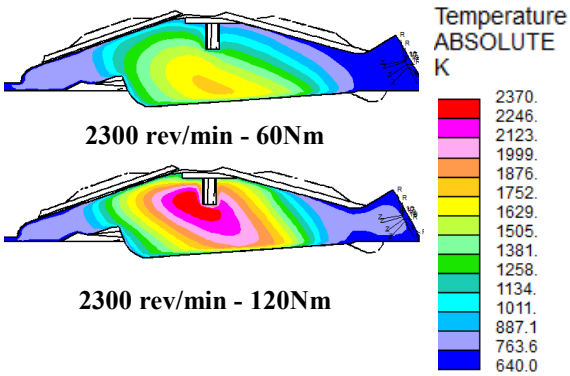

Figure 8. Symmetry plane temperature contours at 10% MFB, for the two operating conditions investigated.

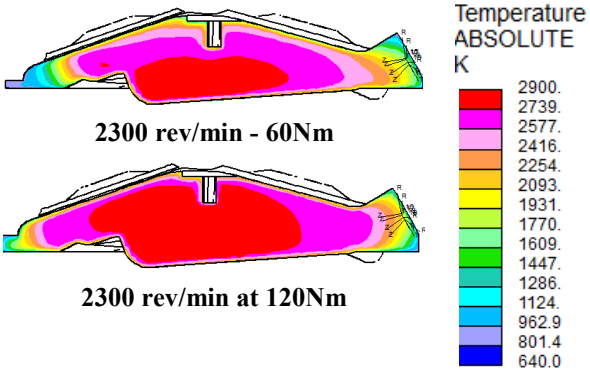

Figure 9. Symmetry plane temperature contours at 90% MFB, for the two operating conditions investigated.

Isomeric views of in-cylinder soot volume fraction are presented in Figure 11. In the higher engine load case, by the end of combustion at 40 CA deg ATDC, the newly formed soot and the amount transported outwardly from the centre, are located mostly in the outer periphery. Here, in spite of the presence of oxygen, the low residence time and the low near-wall temperature reduce the process of oxidation. The strong downward motion created by piston movement midway through expansion keeps the residual soot near the wall at EVO. Figure 11 shows that the soot distribution at lower engine load is rather different. As the flame front sweeps across the chamber, high levels of soot are formed along the dome centreline and in the exhaust valve region. Soot continues to form, supported by poorly mixed fuel, then is pushed outwardly and finally dragged down by the prevailing motion.

Figures 12 and 13 show distributions of molecular oxygen and hydrolix radical OH, in terms of mass fraction. Soot particles and agglomerates are consumed in presence of oxidisers at temperatures above 1400 K. The oxidation process in diesel combustion consumes typically in excess of 90% of the soot mass originally created [32]; stoichiometric combustion in gasoline engines leaves generally little oxygen in the burned gas, hence the overall level of soot oxidation is much lower and strongly dependent on the operating conditions [8, 9, 28]. From 10 CA deg ATDC and on to EVO, the levels of O2 reduce drastically due to the combustion process; higher oxygen concentrations correspond to regions of lower temperature near the walls and vice-versa, an arrangement which is highly unfavourable for particle oxidation. As temperature decreases towards the walls, oxidation is no longer possible, as indicated by the remaining O2 near-wall distribution at EVO. A stronger in-cylinder motion, and the ability to retain this during the expansion stroke, may have a considerable effect on the levels of soot oxidation in gasoline engines running in stoichiometric conditions.

OH radicals form in regions of high temperature (post-flame), are highly reactive and can oxidise soot effectively [8]. Figure 13 shows that high concentrations of OH are located primarily in the core of the chamber, and hence support particle oxidation mostly during the rapid combustion stage. A separate, high-concentration spot forms on the left side of the chamber, possibly as a result of longer residence time of high-temperature burned gas and reduced motion in that region. The low engine load case shows lower gas temperature and lower OH concentrations during combustion up to 40 CA deg ATDC; conversely, the OH concentrations become comparatively higher by EVO, indicating lower soot oxidation in this case.

For brevity, the distributions of soot number density and average size are not presented here. Number density reflects approximately the distribution of soot volume fraction. High bulk gas temperature, in the presence of soot precursor, supports nucleation of new particles and increases

the number. This then reduces in the latter part of combustion not only due to oxidation, but also and importantly due to particle collision and coagulation/agglomeration. The higher engine load case shows lower particle size, mostly due to the effect of late and post-combustion oxidation. The virtually complete absence of oxidation, and the compounded effects of coagulation and surface growth in high number density regions, increase the average size in the lower engine load conditions.

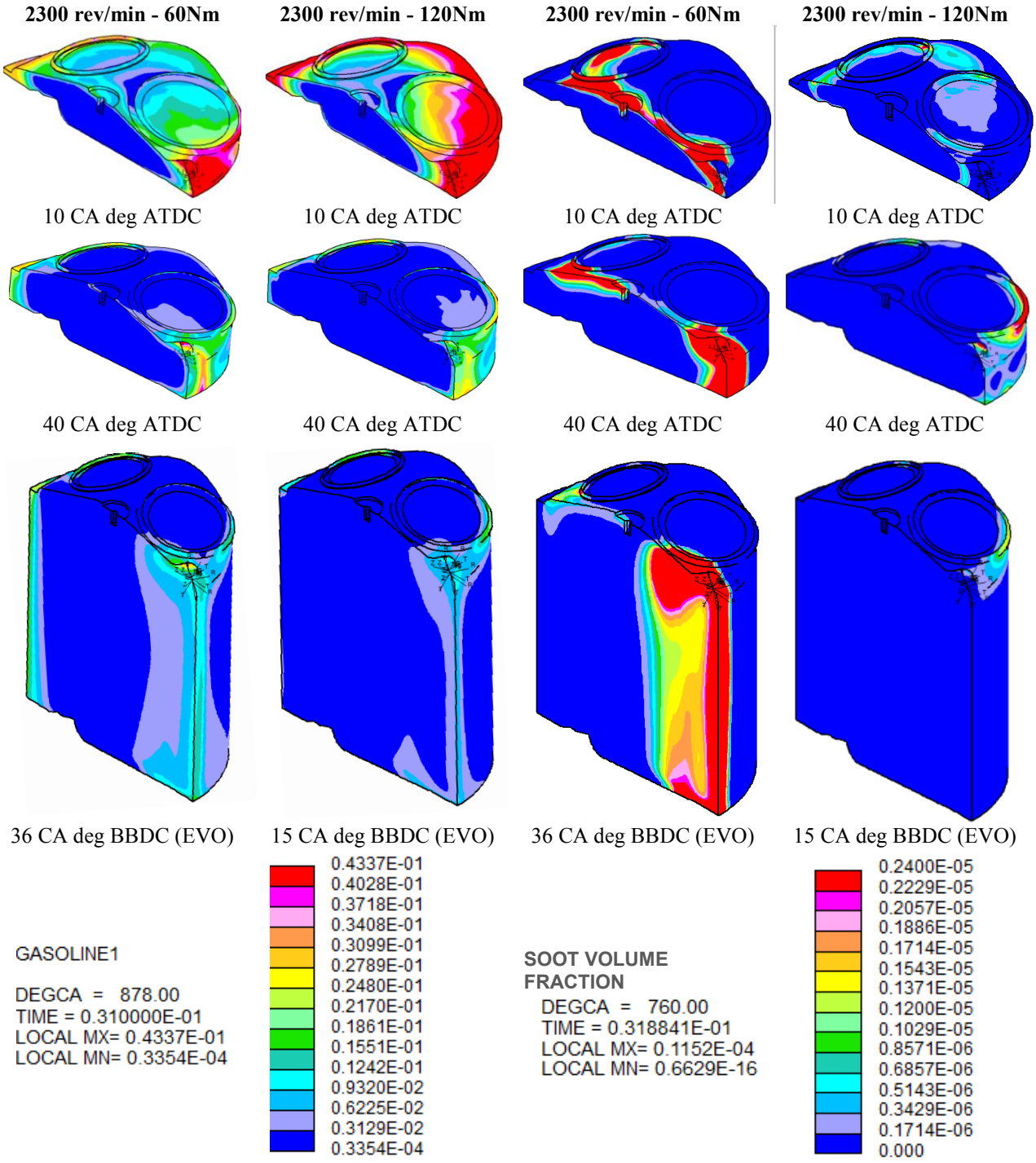

Figure 10. Isomeric views of fuel concentration (mass fraction) at three expansion stroke locations, for the two operating conditions investigated.

Figure 11. Isomeric views of soot volume fraction at three expansion stroke locations, for the two operating conditions investigated.

4. CONCLUSIONS

Through the use of CFD modelling, the present work explores the mechanisms of combustion and soot formation in a modern GDI engine of the wall-guided type. Two part-load engine operating conditions were investigated, 60 and 120 Nm of break torque output at fixed engine speed of 2300

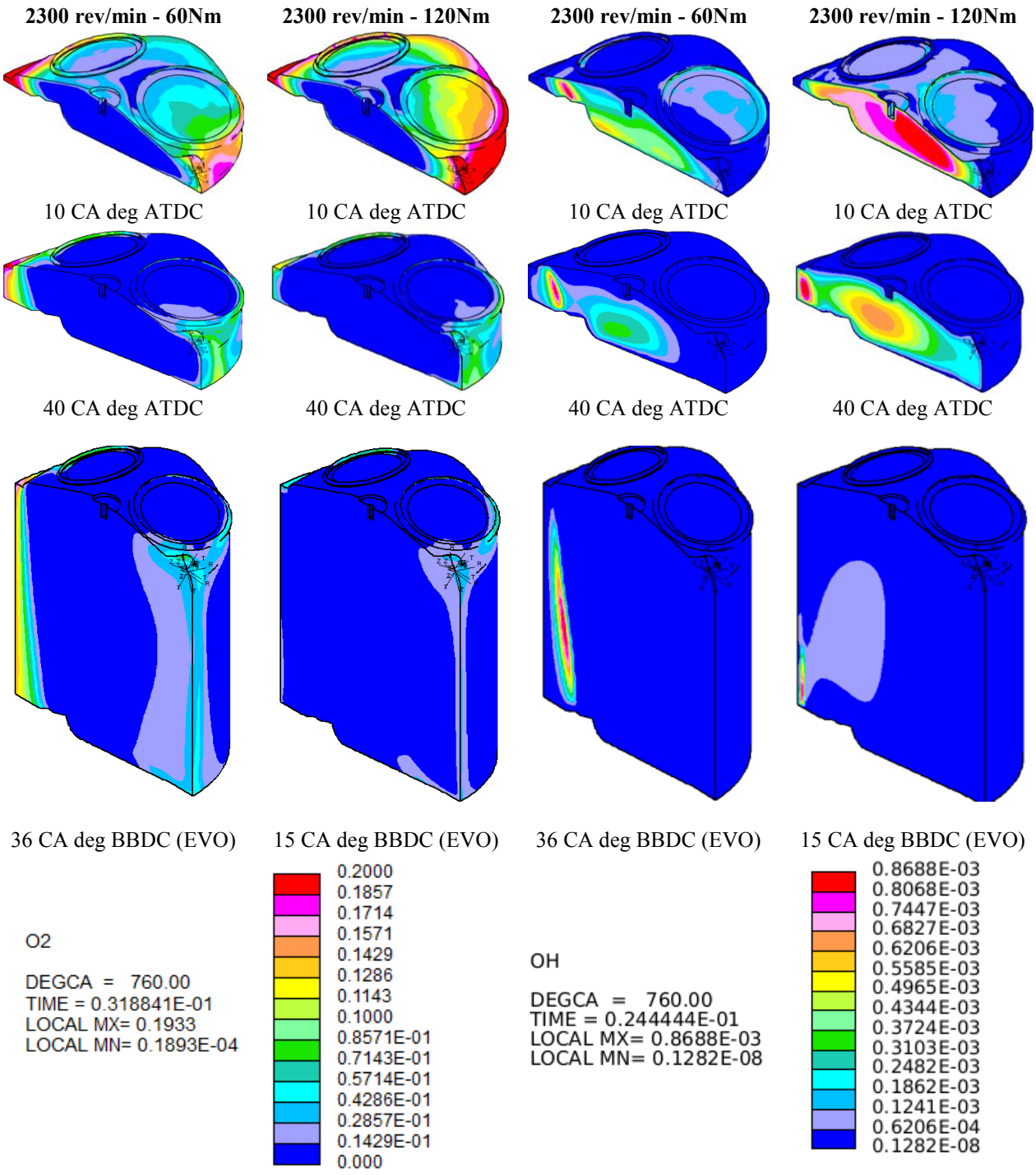

Figure 12. Isomeric views of oxygen concentration (mass fraction) at three expansion stroke locations, for the two operating conditions investigated.

Figure 13. Isomeric views of hydrolix group OH (mass fraction) at three expansion stroke locations, for the two operating conditions investigated.

rev/min. The study aimed to deliver an improved understanding of in-cylinder soot mechanisms with a view to support improved control strategy optimisation; a separate but equally important aim has been to establish potentials and limitations of the current modelling approaches, to facilitate further high-quality research in the field.

The following major conclusions can be drawn from the investigation carried out so far:

- In the steady-state, fully-warm, theoretically-homogeneous, part-load conditions investigated, soot is formed as a result of local mixture stratification; any liquid film formation disappears in all cases before combustion commences.
- The low injection pressure of around 30 bar used at the lower engine load, causes poor fuel droplets atomisation and poor mixture homogeneity at the start and during combustion. In spite of the early intake stroke fuel injection, the resulting equivalence ratio at the time of ignition

shows a wide adverse variation, ranging between 1.4 along the chamber dome and 0.75 over the piston top.

- The high levels of soot measured at lower engine load (three-fold increase in number density compared to the higher load case) are associated to poor mixture preparation, leading to high rates of formation, compounded to very low soot oxidation as a result of, primarily, lower chamber and near-wall temperature.
- The higher engine load case shows much better, near-stoichiometric mixture homogeneity, but also greater bulk gas and near-wall temperature, which supports soot oxidation and increased coagulation/agglomeration, resulting in lower soot mass and number output.
- From about 30 CA deg ATDC onwards, greater O2 concentration corresponds to regions of lower temperature (near the walls) and vice-versa; an arrangement which is unfavourable for effective oxidation.
- Higher concentration of OH appears primarily in the high-temperature core, supporting oxidation mostly during the main combustion event; OH levels are much lower in the lower engine load case.
- The Soot Sectional Method based on available PFR libraries is computationally efficient and can be used effectively to aid the understanding of the complex relations between soot formation and engine in-cylinder conditions. As it stands, the model is not fully "transportable" and requires specific tuning.
- Research work is under-way to establish the relative importance/weight of each soot mechanism, and deliver improved model calibration for GDI combustion.

5. REFERENCES

[1] Bonatesta, F., Altamore, G., Kalsi, J., Cary, M. Fuel economy analysis of part-load variable camshaft timing strategies in two modern small-capacity spark ignition engines. Applied Energy, 164: 475-491, 2016.

[2] Raaschou-Nielsen, O., Andersen, Z. J., Beelen, R., Samoli, E., Stafoggia, M., Weinmayr, G., Xun, W. W. Air pollution and lung cancer incidence in 17 European cohorts: prospective analyses from the European Study of Cohorts for Air Pollution Effects (ESCAPE). The lancet oncology,14(9): 813-822, 2013.

[3] Zhao, F., Lai, M. C., Harrington, D. L. Automotive spark-ignited direct-injection gasoline engines. Progress in energy and combustion science, 25(5): 437-562, 1999

[4] Maricq, M., Podsiadlik, D., Brehob, D., Haghgooie, M. Particulate Emissions from a Direct-Injection Spark-Ignition (DISI) Engine. SAE Technical Paper 1999-01-1530, 1999.

[5] Piock, W., Hoffmann, G., Berndorfer, A., Salemi, P. et al. Strategies Towards Meeting Future Particulate Matter Emission Requirements in Homogeneous Gasoline Direct Injection Engines. SAE Int. J. Engines 4(1):1455-1468, 2011.

[6] He, X., Ratcliff, M. A., Zigler, B. T. Effects of gasoline direct injection engine operating parameters on particle number emissions. Energy & Fuels, 26(4): 2014-2027, 2012.

[7] Hageman, M., Rothamer, D. Sensitivity Analysis of Particle Formation in a Spark-Ignition Engine during Premixed Operation. 8th US National Combustion Meeting, 2013.

[8] Jiao, Q., Reitz, R. Modeling of Equivalence Ratio Effects on Particulate Formation in a Spark-Ignition Engine under Premixed Conditions. SAE Technical Paper 2014-01-1607, 2014.

[9] Jiao, Q., Reitz, R. The Effect of Operating Parameters on Soot Emissions in GDI Engines. *SAE Int. J. Engines*, 8(3): 1322-1333, 2015.

[10] Bonatesta, F., Chiappetta, E., & La Rocca, A., Part-load particulate matter from a GDI engine and the connection with combustion characteristics, Applied Energy, 124: 366-376, 2014.

[11] Star-CD Methodology Manual, Version 4.22, CD-Adapco, 2014.

[12] Malaguti, S., Bagli, G., Montanaro, A., Piccinini, S. et al. Experimental and Numerical Characterization of Gasoline-Ethanol Blends from a GDI Multi-Hole Injector by Means of Multi-Component Approach. SAE Technical Paper 2013-24-0002, 2013.

[13] Rosa, N. G., Villedieu, P., Dewitte, J., Lavergne, G. A new droplet-wall interaction model, Proceedings of the 10th International Conference on Liquid Atomization and Spray System. ICLASS-2006, Japan, 2006.

[14] Semião, V., Andrade, P., da Graca Carvalho, M. (1996). Spray characterization: numerical prediction of Sauter mean diameter and droplet size distribution. Fuel, 75(15): 1707-1714, 1996.
[15] Huang, C., Lipatnikov, A. Modelling of gasoline and ethanol hollow-cone sprays using OpenFOAM. SAE Technical Paper 2011-01-1896, 2011.
[16] Whelan, I. C. A study of particulate matter emissions from gasoline direct injection engines. PhD Thesis, Ireland: National University of Ireland, 2013.
[17] Bonatesta, F., La Rocca, S., Hopkins, E., Bell, D. Application of Computational Fluid Dynamics to Explore the Sources of Soot Formation in a Gasoline Direct Injection Engine. SAE Technical Paper 2014-01-2569, 2014.
[18] Montanaro, A., Allocca, L., Ettorre, D., Lucchini, T., Brusiani, F., Cazzoli, G. Experimental characterization of high-pressure impinging sprays for CFD modeling of GDI engines. SAE International Journal of Engines,4(1): 747-763, 2011.
[19] Lucchini, T., D'Errico, G., Onorati, A., Bonandrini, G., Venturoli, L., Di Gioia, R. Development and application of a computational fluid dynamics methodology to predict fuel-air mixing and sources of soot formation in gasoline direct injection engines. Int. J. Engine Res., published online October 15, 2013.
[20] Yi, Y., De Minco, C. Numerical Investigation of Mixture Preparation in a GDI Engine. SAE Technical Paper 2006-01-3375, 2006.
[21] Bai, C., Gosman, A. Development of Methodology for Spray Impingement Simulation. SAE Technical Paper 950283, 1995.
[22] Malaguti, S., Fontanesi, S., Cantore, G. Numerical characterization of a new high-pressure multi-hole GDI injector. 23rd Annual Conference on Liquid Atomization and Spray Systems, ILASS - Europe 2010, Czech Republic, 2010.
[23] Wang, Y. Validation of an existing mechanism for n-heptane, iso-octane and toluene reference fuels. Brandenburgische Technische Universitat, 2015 [ONLINE] Available at: http://www-docs.tu-cottbus.de/thermodynamik/public/Bachelor_und_Masterarbeiten/Yuting.pdf. [Accessed 15 June 15]
[24] Colin, O., Benkenida, A. The 3-Zone Extended Coherent Flame Model (ECFM3Z) for computing premixed/diffusion combustion, Oil & Gas Science and Technology, 59(6): 593-609, 2004.
[25] Marchal, C. Mod´elisation de la formation et de l'oxydation des suies dans un moteur automobile. PhD Thesis. France: l'université d'Orléans, 2009.
[26] Storch, M., Zigan, L., Wensing, M., Will, S. Systematic Investigation of the Influence of Ethanol Blending on Sooting Combustion in DISI Engines Using High-Speed Imaging and LII. SAE Technical Paper 2014-01-2617, 2014.
[27] Aubagnac-Karkar, D., Michel, J., Colin, O., Noël, L. et al. A Sectional Soot Model for RANS Simulation of Diesel Engines. SAE Technical Paper 2014-01-1590, 2014.
[28] Naik, C., Liang, L., Puduppakkam, K., and Meeks, E. Simulation and Analysis of In-Cylinder Soot Formation in a Gasoline Direct-Injection Engine Using a Detailed Reaction Mechanism. SAE Technical Paper 2014-01-1135.
[29] La Rocca, A., Bonatesta, F., Fay, M. W., Campanella, F. Characterisation of soot in oil from a gasoline direct injection engine using Transmission Electron Microscopy. Tribology International, 86: 77–84, 2015.
[30] Choi, S., Seong, H. Oxidation characteristics of gasoline direct-injection (GDI) engine soot: Catalytic effects of ash and modified kinetic correlation. Combustion and Flame, 162(6): 2371-2389, 2015.
[31] Choi, K., Kim, J., Myung, C. L., Lee, M., Kwon, S., Lee, Y. et al. Effect of the mixture preparation on the nanoparticle characteristics of gasoline direct-injection vehicles. Part D: J Auto 226(11): 1514–24, 2012.
[32] Bonatesta, F., La Rocca, A., Shayler, P. J., Wahab, E. The influence of swirl ratio on soot quantity and distribution in the cylinder of a diesel engine. Third European Combustion Meeting ECM, 2007.